LA-UR- 99-745

*Approved for public release; distribution is unlimited.*

CONF-9810110--

*Title:* Accurate, Finite-Volume Methods for 3D MHD on Unstructured Lagrangian Meshes

*Author(s):* D. C. Barnes and C. L. Rousculp

*Submitted to:* NECDC 98





**Los Alamos**
NATIONAL LABORATORY

## DISCLAIMER

# Accurate, Finite-Volume Methods for 3D MHD on Unstructured Lagrangian Meshes(U)

**D. C. Barnes and C. L. Rousculp**
**Los Alamos National Laboratory**

*Previous 2D methods for magnetohydrodynamics (MHD) have contributed both to development of core code capability and to physics applications relevant to AGEX pulsed-power experiments. This strategy is being extended to 3D by development of a modular extension of an ASCI code. Extension to 3D not only increases complexity by problem size, but also introduces new physics, such as magnetic helicity transport. We have developed a method which incorporates all known conservation properties into the difference scheme on an Lagrangian unstructured mesh. Because the method does not depend on the mesh structure, mesh refinement is possible during a calculation to prevent the well known problem of mesh tangling. Arbitrary polyhedral cells are decomposed into tetrahedrons. The action of the magnetic vector potential,* $\mathbf{A}\cdot\delta\mathbf{l}$*, is centered on the edges of this extended mesh. For ideal flow, this maintains* $\nabla\cdot\mathbf{B}=0$ *to round-off error. Vertex forces are derived by the variation of magnetic energy with respect to vertex positions,* $\mathbf{F}=-\partial W_B/\partial\mathbf{r}$*. This assures symmetry as well as magnetic flux, momentum, and energy conservation. The method is local so that parallelization by domain decomposition is natural for large meshes. In addition, a simple, ideal-gas, finite pressure term has been included. The resistive diffusion part is calculated using the support operator method, to obtain an energy conservative, symmetric method on an arbitrary mesh. Implicit time difference equations are solved by preconditioned, conjugate gradient methods. Results of convergence tests are presented. Initial results of an annular Z-pinch implosion problem illustrate the application of these methods to multi-material problems. (U)*

**Keywords:** Magneto-hydrodynamics, Z-pinch, Lagrangian Unstructured-mesh

## Introduction

The magneto-hydrodynamical (MHD) approximation is applicable to a wide variety of plasma environments, including pulsed power experiments. Numerical modeling is essential for the understanding of such an environment because limited diagnostics and the cost of involved in single experiment.

MHD is naturally three-dimensional (3D) (Biskamp 1993). Up til now, most computational treatments have been one or two dimensional (1D,2D) out of economic necessity. However, because of the exponential increase in computing power in the last decade, full 3D computations are now possible on workstations rather than mainframe supercomputers. This means that it is now possible to extensively investigate MHD phenomenea that manifest only in three-dimensions.

With the added dimsionallity comes added complexity. It is easy to assume that 2D methods carry over to 3D simply by changing geometric constructs. One such potential problem is when surface normal vectors to a computational cell are used. In 2D, surface normals are well defined either in the plane by the normal to the line connecting two vertices or as perpendicular to the plane. In 3D however, a surface normal is only well defined for a surface described by three points, since only three points are necessarliy coplaner. Therefore, a 2D method that relies on anything, but triangular computational cells, will be ill defined in 3D.

## Mathematical Model

We consider here the single fluid, approximation to MHD (Polovin and Demutskii 1990). The relevent equations in Lagrangian form are,

$$\frac{d\rho}{dt} = -\nabla \cdot \mathbf{v} \tag{1}$$

$$\rho \frac{d\mathbf{v}}{dt} = \mathbf{J} \times \mathbf{B} - \nabla p \tag{2}$$

$$\frac{d\mathbf{B}}{dt} = (\mathbf{v} \cdot \nabla)\mathbf{B} - \nabla \times \mathbf{E} \tag{3}$$

$$\mathbf{E} = -\mathbf{v} \times \mathbf{B} + \eta \mathbf{J} \tag{4}$$

$$\mu_0 \mathbf{J} = \nabla \times \mathbf{B}. \tag{5}$$

$$p = p_0 (\frac{V_0}{V})^{\gamma}. \tag{6}$$

Here $\rho$ is the plasma mass density; $\mathbf{B}$ is the magnetic field; $p$ is the fluid pressure; $\mathbf{v}$ is the fluid velocity; $\mathbf{J}$ is the electric current density; $\mathbf{E}$ is the electric field; and $\mu_0$ is the permeability of free-space. Eqn. 1 is conservation of mass equation. Eqn. 2 is conservation of momentum equation. Eqn. 3 is Faraday's Law. The first term on the right-hand-side comes from the definition of the material derivitive $[d/dt = \partial/\partial t + (v \cdot \nabla)]$. Eqn. 4 is Ohm's Law for an resitive conducting fluid, where $\eta$ is the resistivity of the fluid. Eqn. 5 is Ampere's Law for low frequencies ($\omega/\omega_{pe} < 1$, $\omega_{pe}$ is the electron plasma frequency). Eqn. 6 is the isentropic, gamma-law eqation of state, where $\gamma$ is ratio of specific heats.

For an infinte, uniform ($\rho = const$) plasma, in the ideal case ($p = 0$ and $\eta = 0$), the above equations may be linearized [$\mathbf{v}(\mathbf{r},t) \rightarrow \mathbf{v_1}(\mathbf{r},t)$ and $\mathbf{B}(\mathbf{r},t) \rightarrow \mathbf{B_0} + \mathbf{B_1}(\mathbf{r},t)$], Fourier transformed ($d/dt \rightarrow -i\omega, \nabla \rightarrow i\mathbf{k}$), and combined to give a dispersion realation for the normal wave modes. The dispersion relation is

$$\omega^2 \mathbf{v}_1 = v_A [k_{||}^2 \mathbf{v}_1 - k_{||}(\mathbf{k} \cdot \mathbf{v}_1)\mathbf{b} - k_{||}(\mathbf{b} \cdot \mathbf{v}_1)\mathbf{k} + (\mathbf{k} \cdot \mathbf{v}_1)\mathbf{k}], \tag{7}$$

where $v_A = B/\sqrt{\mu_0 \rho}$ is the Alfven velocity, $\mathbf{b} = \mathbf{B}_0/B_0$ is a unit vector in the direction of the background magnetic field, and $k_{||} = \mathbf{k} \cdot \mathbf{b}$ is the parallel component of the wave vector, $\mathbf{k}$.

The two eigenvalues/freqencies of Eqn. 7 are

$$\omega^2_{fast} = v_A^2 k^2 \quad (8)$$

$$\omega^2_{shear} = v_A^2 k_{||}^2, \quad (9)$$

with positive/negative roots of each $\omega^2$ corresponding to backward/forward traveling mode. The associated polarizations or eigenvectors are

$$\mathbf{v}_{fast} = \mathbf{k}_\perp \quad (10)$$

$$\mathbf{v}_{shear} = \mathbf{k} \times \mathbf{b}. \quad (11)$$

A third mode, the slow mode, is non-propagating in the $\beta = p/(B^2/2\mu_0) = 0$ limit. For finite $\beta$, it becomes the the slow magneto-sonic wave. The two non-zero modes are the fast magneto-sonic wave and the shear wave. Their frequencies can differ in value by several orders of magnitude, if $k$ is highly oblique ($k_{||}/k << 1$).

Discretization errors of the ideal equations can lead to the phenomenea of spectral pollution. In Fig. 1, $\omega_{fast}$ and $\omega_{shear}$ are plotted as a function of wave vector angle for $k = const$. It is seen that for a highly oblique angle, $\omega_{fast} \gg \omega_{shear}$. In the discritized case, the value of $\omega_{shear}$ is increased or polluted by the value of $\omega_{fast}$. In an inhomogeneous ($\rho \neq const$) or non-infinite geometry, oscillations can become instabilites when the frequencies are imaginary ($\omega^2 < 0$). Since instabilities eventually dominate the dynamics of a particular configuration, discretization errors can lead to non-physical numerical solutions. Hence, if a MHD method is to be robust for different plasma geometries and conditions, a dicretization method free of spectral pollution is essential. The finite volume method described in the following section meets this requirement.

In the highly resitive limit ($\eta \gg \mu_0 v_A/k$, i.e. low Lundquist number), but still with $p = 0$, the fluid remains motionless ($\mathbf{v} = 0$), while the magnetic field diffuses though it. The reduced equations are

$$\frac{d\mathbf{B}}{dt} = -\nabla \times \mathbf{E} \quad (12)$$

$$\mathbf{E} = \frac{\eta}{\mu_0} \nabla \times \mathbf{B}. \quad (13)$$

These equations (with the $\nabla \cdot \mathbf{B} = 0$) can be combined into a single vector diffusion equation. However, the above form emphisizes that the two curl operators have different domains and ranges, which is readily apparent in the discretized case, where $\mathbf{B}$ and $\mathbf{E}$ do not have the same centering. The important property of these equations is the adjoint relation between the two curl operators. This property must be preserved in the discretized case if accurate results are desired (Shashkov and Steinberg 1996).

## Mesh

A 3D, unstructured mesh is employed in our method. The vertices are stored as a simple linear array of points. Computational cells can have an arbitrary number of faces and these faces can

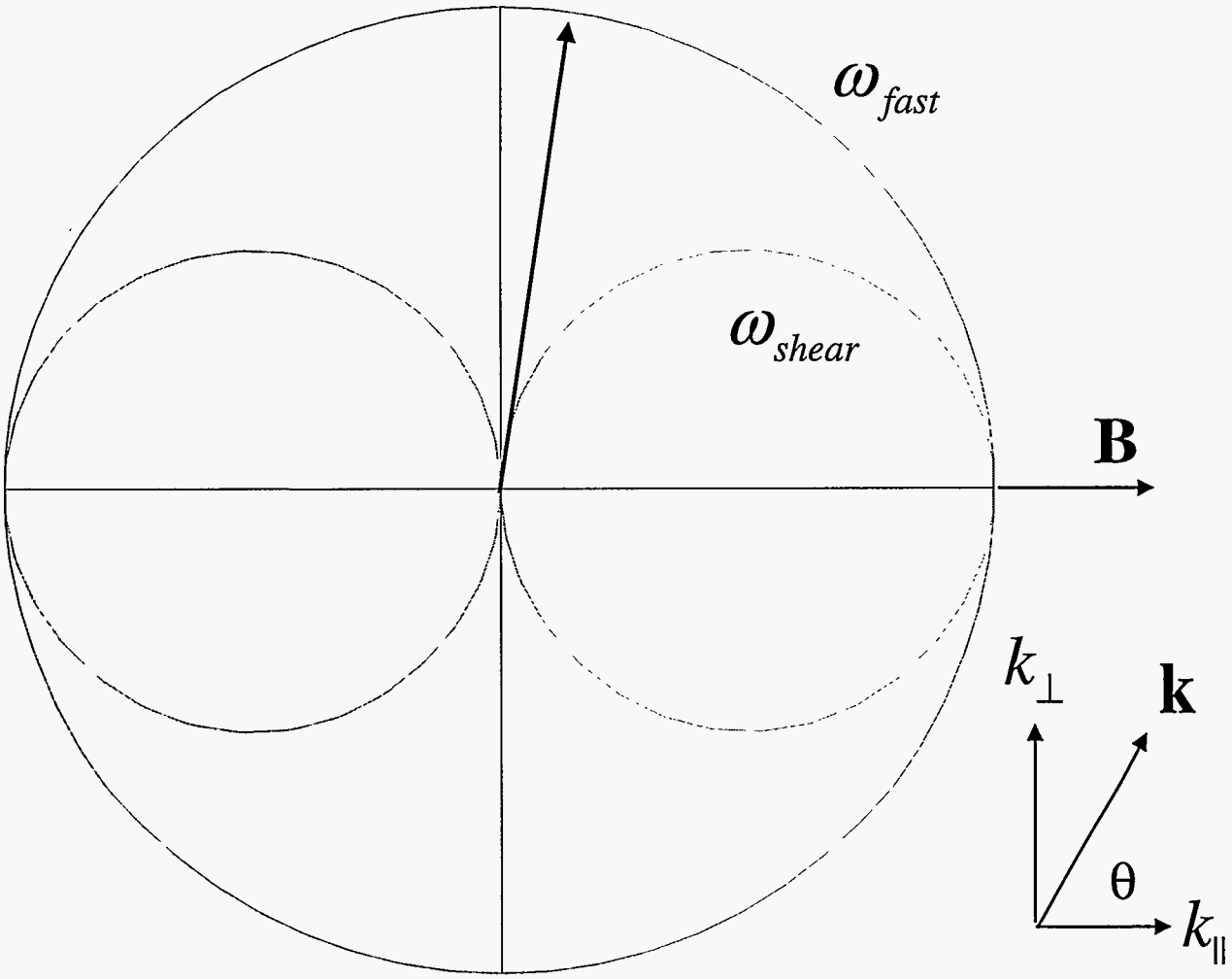


Figure 1: Disperion relations for the fast and shear MHD modes as a function of the angle of $k$. For highly oblique angles (black line), $\omega_{fast} \gg \omega_{shear}$ which can lead to spectral pollution.

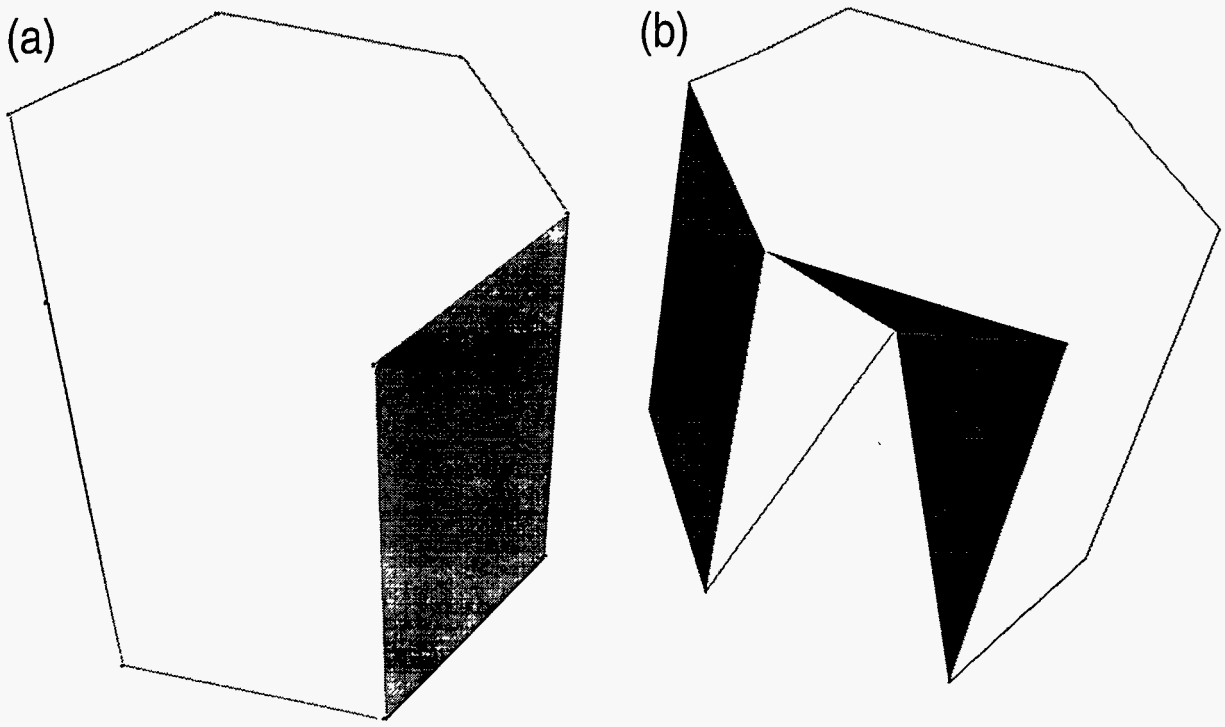


Figure 2: (a) An eight faced computational cell. (b) Decompositon of the cell into 36 unique tetrahedrons. Four tetrahedrons are remove to show the interior.

have an arbitrary number of edges. A diagram of a eight faced cell is shown in Fig. 2(a). Fortran 90 data types for the cells and faces are defined. A single cell consists of an allocatable array of indices of faces, while a single face consists of an allocatable array of indices of vertices. For each cell and face the geometric center is computed and added to the list of vertices. By then connecting the original cell vertices to the cell center, and the face vertices to the face center, the cell is decomposed into a set of tetrahedrons (tets). This decomposition is shown in Fig. 2(b). In a single cell, the number of unique, non-overlapping tets is $n_{tets} = \sum_{if=1}^{nf} ne_{if}$, where $nf$ is the number of faces that make up the cell, and $ne_{if}$ is the number of edges of a face. For the eight-faced cell in Fig. 2, there are 36 tets per cell. For a standard six-faced, rectangular hexahedron there are 24 tets per cell. While the cell vertices are updated by the equation of motions, each computational cycle, the cell and face centers are forgotten then recomputed geometrically each cycle. Note that the vertex mass, $m$, is a constant in time because of the Lagrangian dynamics formulation. The limitation on the original mesh is that each cell have positive initial volume and that the cell center be located within the cell. At this point, the meshing algorithm is not smart enough to recognize degenerate hexahedral cells (prisms, pyrimids, or tets) in the original mesh and so will decompose them unnecessarily. However, degenerate hexahedral cells do not place a restriction on the differencing scheme.

## Differencing Scheme

**Ideal.** The finite volume differencing of the MHD equations is described here. The method is Lagrangian; this means that the mesh verticies move with the magneto-fluid flow. The method is explicit so that, $\mathbf{x}^{t+1} = \mathbf{f}^t(\Delta t)^2/m + 2\mathbf{x}^t - \mathbf{x}^{t-1}$. The magnetic vector potential ($\mathbf{A}$, such that $\nabla \times \mathbf{A} = \mathbf{B}$) is introduced. It is stored as an edge-centered scalar $A_{ie} = \mathbf{A} \cdot \mathbf{l}$, where $\mathbf{l}$ is a vector directed along an edge connecting two vertices. In terms of the tetrahedral mesh, the quantity is defined on every unique edge of a tetrahedron, as indicated by the subscript *ie*. For each face of a tetrahedron, a magnetic flux is defined in terms of $A_{ie}$, by the discrete form of Stoke's theorem, $\Phi_{if} = \sum_{ie=1}^{3} A_{ie}$. Fig. 3 shows the centering of the variables in a single tetrahdron. If $\mathbf{A}$ is initialized such that $\nabla \cdot \mathbf{B} = 0$, then it will remain for the entire caclulation since $dA_{ie}/dt = 0$, which implies $d\Phi_{if}/dt = 0$.

In terms of these quantities, magnetic forces, $\int dV \mathbf{J} \times \mathbf{B}$, are calculated at each of the dynamical vertices using a finite volume approximation.

$$\mathbf{f}_{iv} \propto \sum_{it \in iv} B_{iz}^2 \mathbf{s}_{it} - \mathbf{B}_{if} \Phi_{if}, \tag{14}$$

where $\mathbf{f}_{iv}$ is force on vertex, *iv*. $B_{iz}^2$ is a zone centered approximation to the magnetic energy. $\mathbf{s}_{if}$ is a directed surface of tetrahedron, *it*. $\mathbf{B}_{if}$ is a face centered approximation of the magnetic field. The sum is over all tets that contain vertex, *iv*. The first term in Eqn. 14 represents magnetic pressure. Consequently, $B_{iz}^2 \rightarrow B_{iz}^2 + p_{iz}$ for non-zero fluid pressure. The second term in Eqn. 14 is unique to MHD and represents forces generated by curvature of magnetic field lines.

**Diffusion.** The resistive diffusion, Eqn. 12 is handled by an implicit, pre-conditioned Conjugate-Gradient (CG) solver (Saad 1996). The method is symmetric and postitive definite, which ensures energy conservation. It also preserves flux conservation so that $\nabla \cdot \mathbf{B} = 0$.

## Numerical Examples

**MHD Modes.** A $10 \times 10 \times 10$ hexahedral cell mesh is generated. The mesh spacing is $\Delta x = \Delta y = 0.1$ m and $\Delta z = 1$ m. A $\mathbf{B}_0 = 1$ V·s/m$^2$ is aligned along the $z-$axis with uniform mass density of $\rho = 3 \times 10^{-7}$kg m$^{-3}$. This gives an Alfven velocity, $v_A = 1.629 \times 10^6$ m/s. A wave vector of $\mathbf{k} = 2\pi(1, 0, 0.1)$ (single oscillation in $x$ and $z$ directions) gives an obliqueness factor of $k_{||}/k = 0.099$ or an angle between $\mathbf{k}$ and $\mathbf{b}$ of $\theta = \cos^{-1}(k_{||}/k) = 84.3°$. Boundary conditions are periodic in all three dimensions. Explicit time-stepping is used so that $\Delta t = 1 \times 10^{-8} < min(\Delta x, \Delta y, \Delta z)/v_A$. This setup is shown in Fig. 4.

In order to generate a standing fast magneto-sonic wave, $\mathbf{v}_x = \mathbf{k}_\perp$ is set with a sinusoidal spatial distribution with a maximum value of $10^{-3} v_A = 1.629 \times 10^3$ m/s. In the top-left inset of Fig. 4, a plot of $v_x$ at the origin over time shows a perfect sinusoidal oscillation within one percent of the theoretically predicted fast wave frequency, $\omega_{fast} = v_A k = 9.65 \times 10^8$ s$^{-1}$.

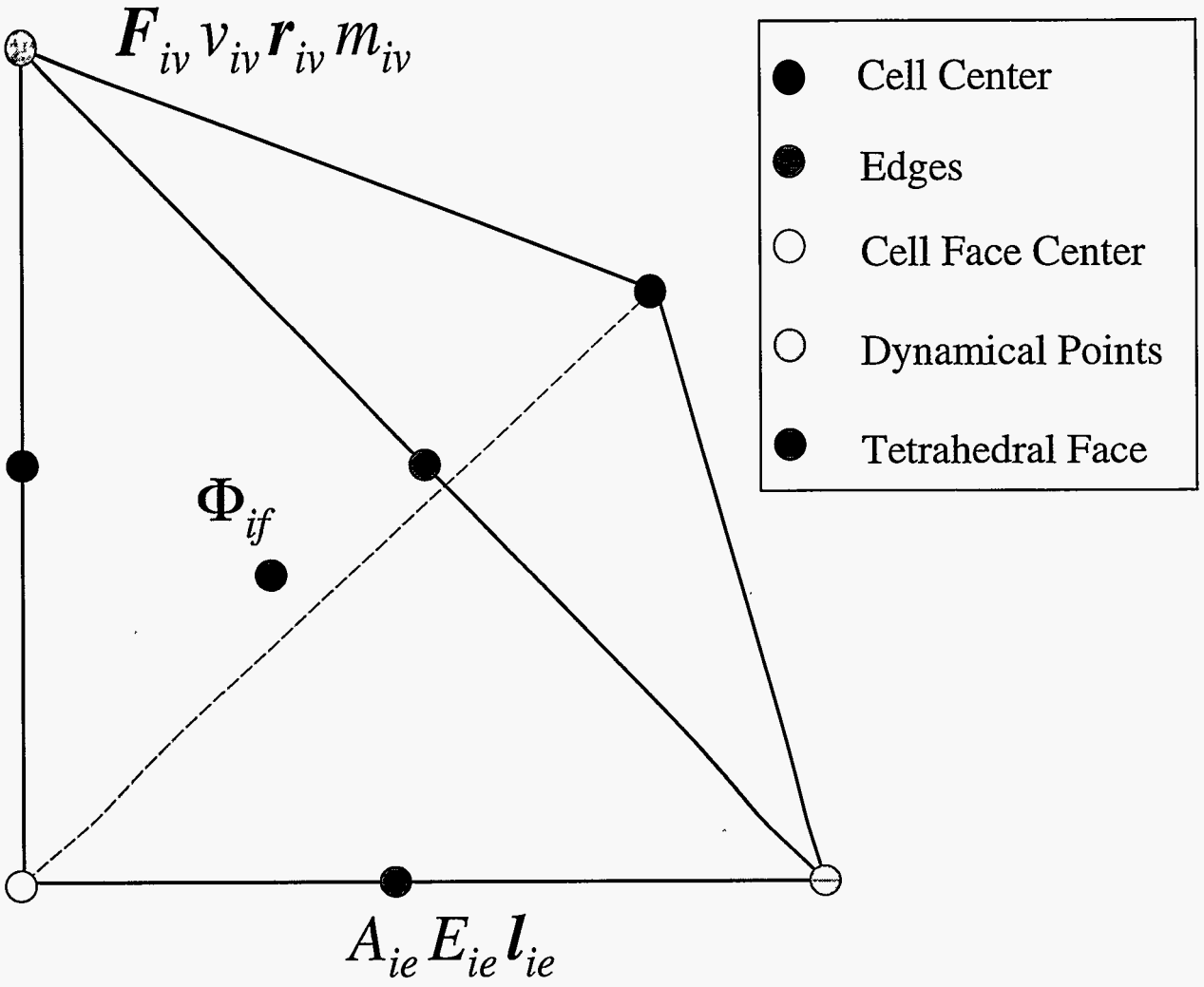


Figure 3: A tetrahdon with the edge-centered (red dots) vector potential $A_{ie}$, electric field $E_{ie}$, and edge length, $\mathbf{l}_{ie}$. The magnetic flux, $\Phi_{if}$ is centered at the face of a tet (blue dot). The force, velocity, position and mass, $\mathbf{F}_{iv}, \mathbf{v}_{iv}, \mathbf{r}_{iv}, m_{iv}$, are located at the dyamical points (green dots). The cell center (black dot) and cell face center (yellow dot) are also shown.

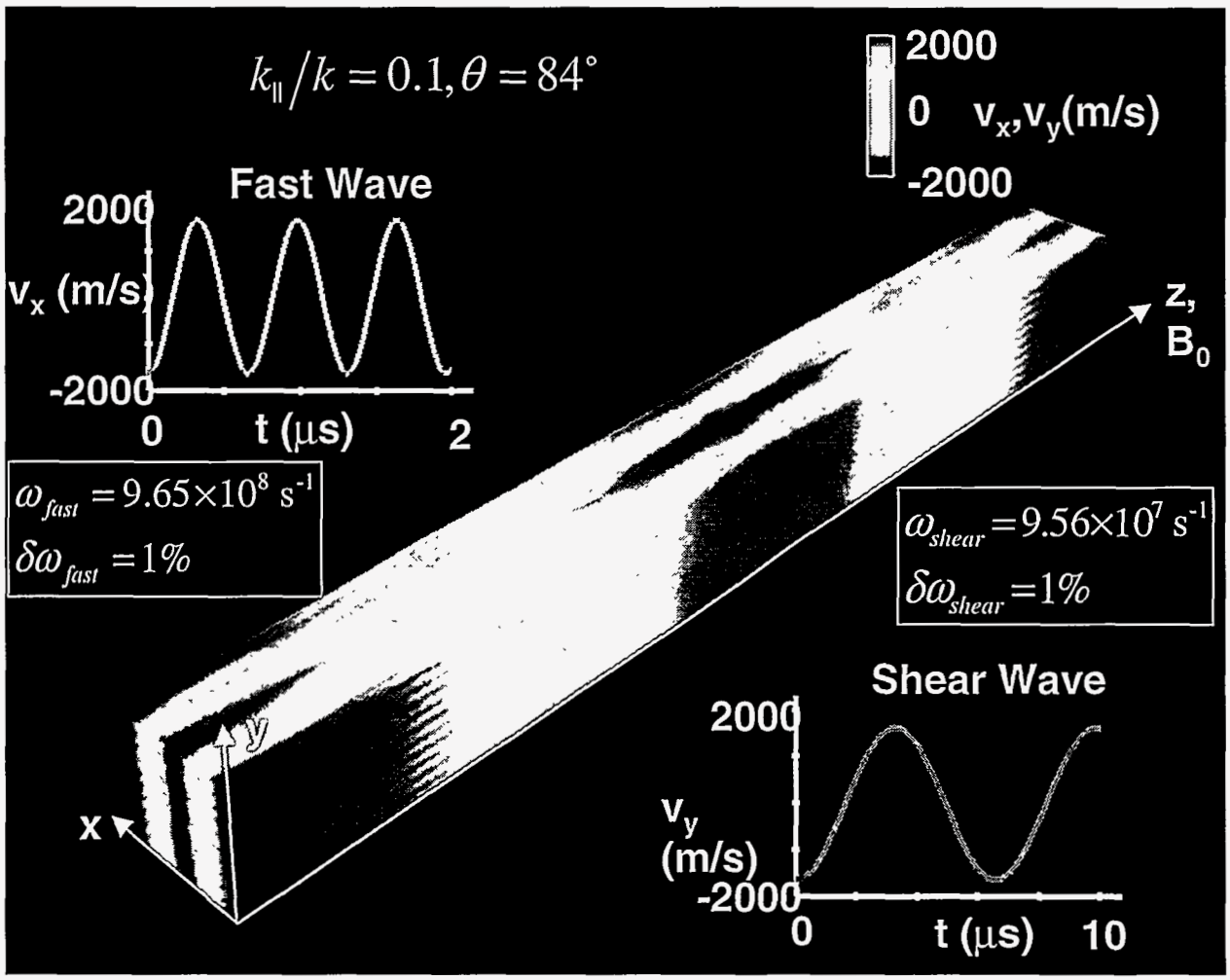


Figure 4: A $10 \times 10 \times 10$ hexahedral cell mesh with a 10:1 aspect ratio is generated. Either $v_x$ or $v_y$ is set with the sinusoidal standing wave pattern to give either a fast or shear polarization of a highly oblique wave vector. The other components of **v** are set to zero. The top-left inset is a plot of $v_x$ for the fast wave polarization, at the origin. Over time it shows a perfect sinusoidal oscillation within one percent of the theoretically predicted fast wave frequency, $\omega_{fast} = v_A k = 9.65 \times 10^8$ s$^{-1}$. The bottom-right inset is a plot of $v_y$ for the shear wave polarization, at the origin. Over time it shows a perfect sinusoidal oscillation within one percent of the theoretically predicted shear wave frequency, $\omega_{shear} = v_A k_{||} = 9.56 \times 10^7$ s$^{-1}$.

In order to generate a standing shear wave, $v_y = \mathbf{k} \times \mathbf{b}$ is set with a sinusoidal spatial distribution with a maximum value of $10^{-3} v_A = 1.629 \times 10^3$ m/s. In the lower-right inset of Fig. 4, a plot of $v_y$ at the origin over time shows a perfect sinusoidal oscillation within one percent of the theoretically predicted fast wave frequency, $\omega_{shear} = v_A k_{||} = 9.56 \times 10^7$ s$^{-1}$.

**Z-pinch.** This methods are applicable to the modeling of pulsed power experiments. Specifically, multi-material, magnetically-driven, liner implosions. In this geometry, the plasma is unstable since the radial force does not serve to straighten the azimuthal magnetic field lines (Biskamp 1993). Fig 5 shows a model of a multi-material ($\rho_{inner} = 5.69\rho_{outer}$) annular liner undergoing this instability. A constant current in the z-direction is applied. Vectors show the azimuthal magnetic field as well as the radial velocity.

**Diffusion.** A unit hexahedral mesh is constructed with unit aspect ratio. It is given a sinusoidal perterbation ($r_{perturb} = r_0 \sin(\pi x) \sin(\pi y)$), where $r_0$ is the magnitude of the pertubation, in the z-direction. The plasma has $\rho = 3 \times 10^{-7}$kg m$^{-3}$ and $\eta = 5 \times 10^{-8}$ ($\Omega$ s)$^{-1}$. At time $t = 0$, $\mathbf{B} = 0$ inside the mesh. An electric field $\mathbf{E} = \eta/\mu_0(x, -y, 0)$ is applied on the x,y boundaries, while the problem is periodic in the z-direction. After 15 s, the magnetic field has diffused into volume and asymtotically approaches the analytic solution, $B_z = 2xy$. In Fig. 6, the smoothly perturbed mesh is shown colored with the value of $B_z$. The inset of Fig. 6 shows the time evolution of the $B_z$ at the point (-0.5,-0.5,0.0).

Results of convergence studies of the diffusion method are shown in Fig. 7. The unit mesh, metioned above, is refined from $5^3$ to a $10^3$ to a $20^3$. A root-mean-square (RMS) error from the analytic solution are calculated and a log-log plot versus the number of cells in one dimension (5,10,10). Fig. 7(a) shows that the method is 2nd order convergent for the smoothly perturbed mesh. A similar unit mesh is constructed, only the perturbation of each vertex is randomized and normalized to the intermesh spacing. Once again, the mesh is refined and an RMS error from the analytic solution is plotted. In Fig. 7(b) the convergence is shown to be only first order.

## Conclusions

Finite-volume, MHD methods for use in single fluid plasma approximation has been demonstrated. In the ideal case, the fast and shear waves have been accurately modeled and show no spectral pollution. An numerical example was given to show how this method could be used to model multi-material, pulsed-power, liner implosions. In the resitive case, the method is second-order convergent on a smoothly perturbed mesh, while it is first-order convergent on a randomly perturbed mesh. The method utilizes an unstructured mesh where computational cells can be composed of any number of faces and faces can be composed of any number of vertices. Because these MHD methods are not based on mesh structure, they can easily be incorporated as a module in the ASCI Shavano Project.

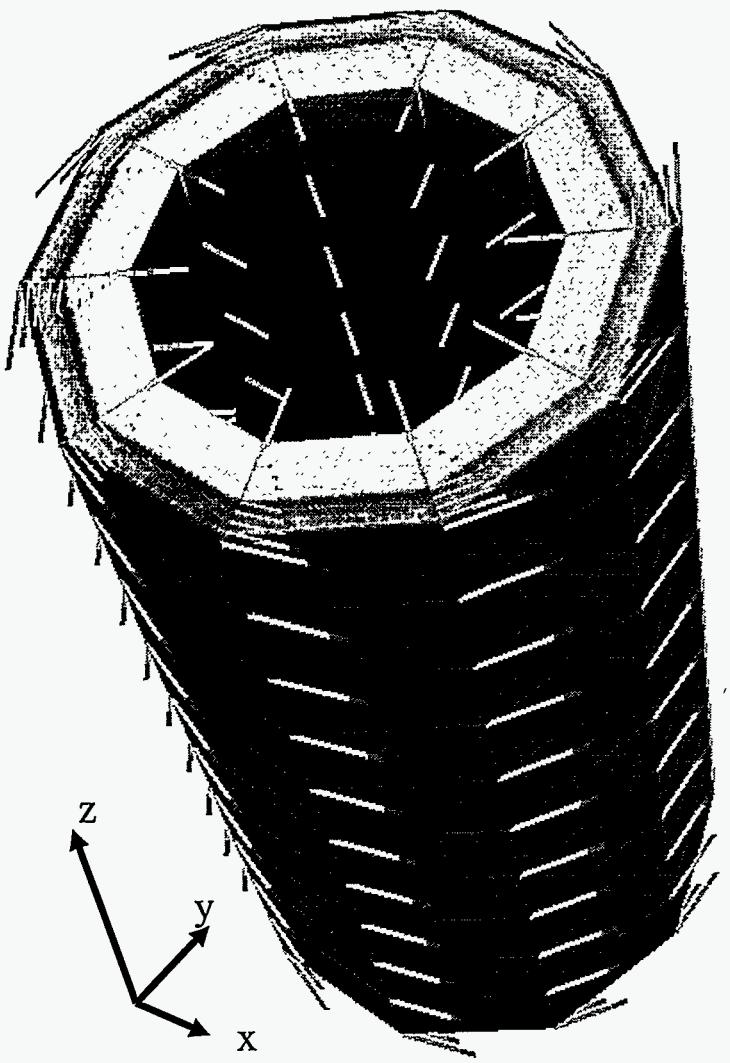


$$\mathbf{B} = B_0\left(r - \frac{r_0^2}{r}\right)\hat{\theta}$$

$$\mathbf{J} = \frac{\nabla \times \mathbf{B}}{\mu_0} = \frac{2B_0}{\mu_0}\hat{z}$$

$$\mathbf{F} = -JB\hat{r}$$

Figure 5: A mulit-material annular liner subjected to a constant axial current density. The magnetic field is azimuthal, while the velocity is radially inward.

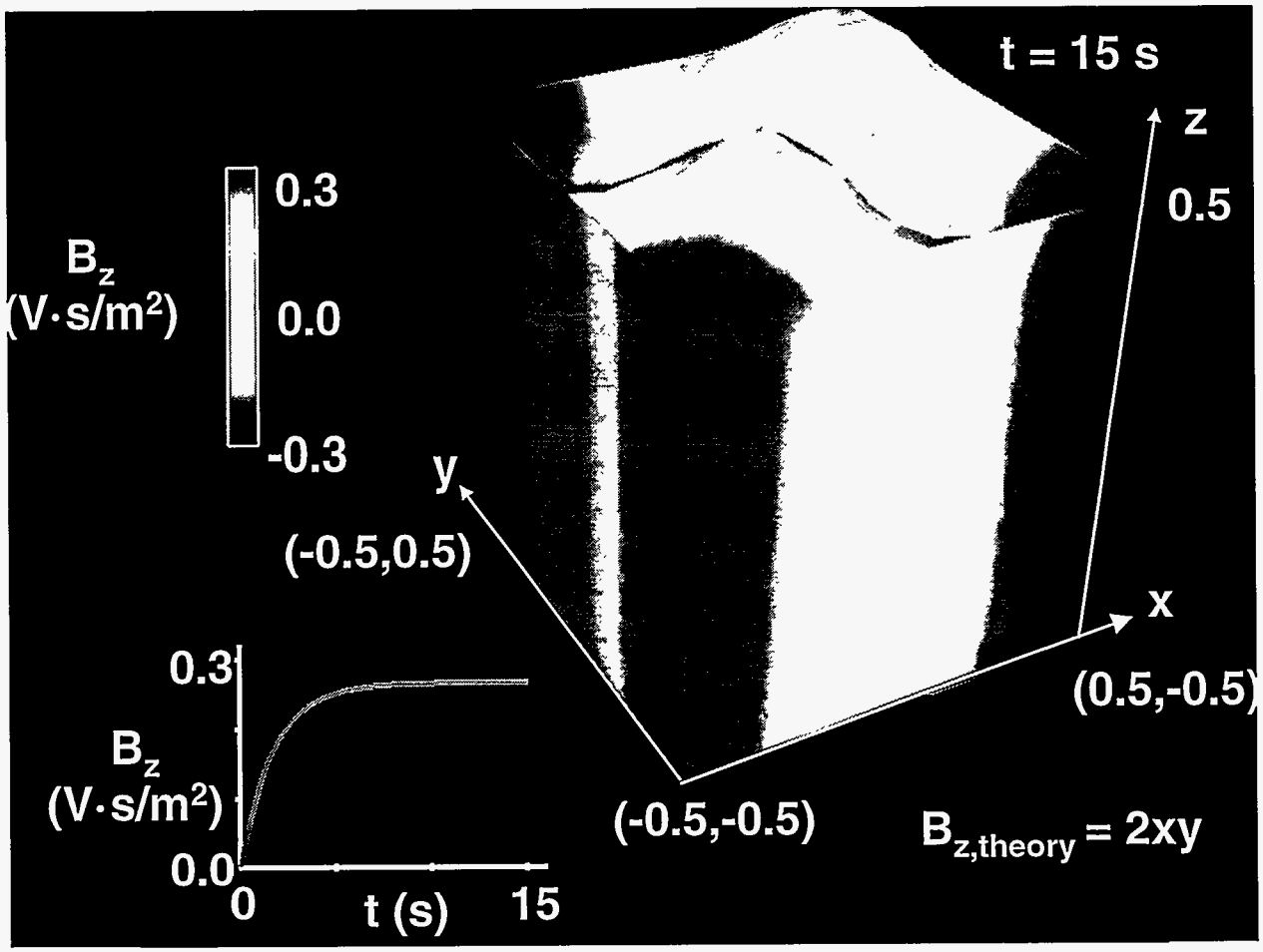


Figure 6: The diffusion of the magnetic field into a unit test volume. The analyitc solution is $B_z = 2xy$. The inset shows the time evolution of $B_z$ at the point (-0.5,-0.5,0.0).

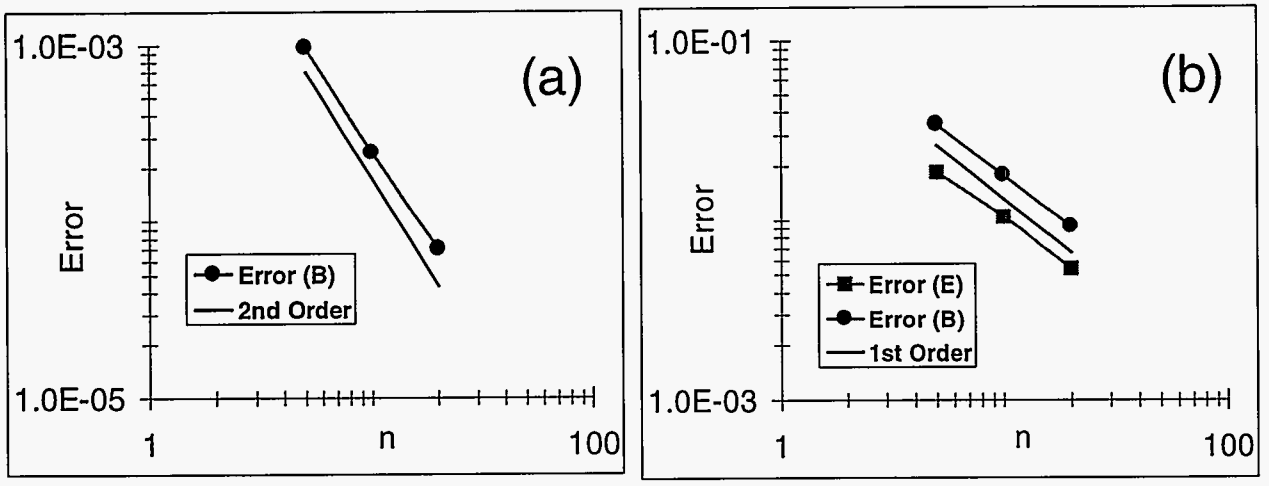


Figure 7: Results of convergence studies for (a) a smoothly perturbed mesh and (b) a randomly perturbed mesh. Errors are RMS from the analytic solution $B_z = -2xy$. $n$ is the number of cells in one dimension (5,10,20).

## References


Biskamp, D. (1993). *Nonlinear Magnetohydrodynamics*. Great Britian: Cambridge University Press.

Polovin, R. V. and V. P. Demutskii (1990). *Fundamentals of Magnetohydrodynamics*. New York: Consultants Bureau.

Saad, Y. (1996). *Iterative Methods fo Sparse Linear Systems*. Boston: PWS Publishing Company.

Shashkov, M. and S. Steinberg (1996). *Conservative finite-difference methods on general grids*. Boca Raton: CRC Press.